AGU PUBLICATIONS

JGR

Journal of Geophysical Research: Atmospheres

RESEARCH ARTICLE
10.1002/2016JD024923

Key Points:
- We use CO as a tracer for incomplete combustion to study pollutant transport to the Arctic
- We find a persistent decrease in surface CO concentrations and a progressively dampened seasonal cycle at three Arctic sites
- We use an atmospheric chemistry transport model to link observations to decreasing European and North American fossil fuel emissions of CO

Correspondence to:
A. R. Mackie,
anna.mackie@ed.ac.uk

Citation:
Mackie, A. R., P. I. Palmer, J. M. Barlow, D. P. Finch, P. Novelli, and L. Jaeglé (2016), Reduced Arctic air pollution due to decreasing European and North American emissions, *J. Geophys. Res. Atmos.*, *121*, 8692–8700, doi:10.1002/2016JD024923.

Received 10 FEB 2016
Accepted 24 JUN 2016
Accepted article online 12 JUL 2016
Published online 22 JUL 2016

Reduced Arctic air pollution due to decreasing European and North American emissions

Anna R. Mackie[1], Paul I. Palmer[1], James M. Barlow[1], Douglas P. Finch[1], Paul Novelli[2], and Lyatt Jaeglé[3]

[1]School of GeoSciences, University of Edinburgh, Edinburgh, UK, [2]NOAA ESRL Global Monitoring Division, Boulder, Colorado, USA, [3]Department of Atmospheric Sciences, University of Washington, Seattle, Washington, USA

Abstract Atmospheric transport of midlatitude pollutant emissions to the Arctic can result in disproportionate impacts on the receptor region. We use carbon monoxide (CO), a tracer of incomplete combustion, to study changes in pollutant transport to the Arctic. Using a wavelet transform, we spectrally decompose CO mole fraction measurements from three Arctic sites (Alert, Barrow, and Zeppelin) collected by NOAA over the past 20–25 years. We show that CO concentrations have decreased by −1.0 to −1.2 ppb/yr. We find that the dampened seasonal cycle (−1.2 to −2.3 ppb/yr) is mostly due to a reduction in peak concentrations (−1.5 to −2.4 ppb/yr), which we attribute to reduced source emissions. We find no evidence to support a persistent increase in hydroxyl radical concentration. Using the GEOS-Chem global 3-D chemistry transport model, we show that observed decreases are consistent with reductions in fossil fuel usage from Europe and North America.

1. Introduction

Observed increases in Arctic surface air temperatures are larger than the global mean average and are projected to increase rapidly over the current century [*Stocker et al.*, 2013]. These increases are due to increasing concentrations of long-lived greenhouse gases whose perturbations to Earth's radiation balance are exacerbated by positive feedback mechanisms. However, air pollution mainly comprised of short-lived gases and particulate matter also significantly affects Arctic climate via changes to, for example, surface albedo and cloud optical properties, involving physical and chemical processes for which current knowledge is incomplete [*Stocker et al.*, 2013].

We use atmospheric CO as a proxy for midlatitude combustion pollutant sources and focus on observed variations. However, we acknowledge that CO and particulate matter will be subjected to different physical and chemical processes that will ultimately determine their transport efficiency. The importance of tropospheric CO lies in its role as a sink for the hydroxyl radical (OH), the main tropospheric oxidant for many air pollutants. Given sufficient nitrogen oxides, CO is a precursor of tropospheric ozone [*Derwent et al.*, 1998], which itself has an enhanced shortwave radiative forcing effect in the Arctic [*Shindell*, 2007]. CO has a large direct source from combustion and a large, diffuse indirect source from the oxidation of methane and nonmethane volatile organic compounds. Atmospheric loss of CO is due primarily to oxidation by OH, resulting in a lifetime of several weeks to a few months depending on the availability of sunlight and water vapor determined by latitude and season. The resulting seasonal cycle for CO at high-latitude peaks in late winter/early spring due to variations in atmospheric transport fluxes from midlatitude sources and a minimum during summer months when the OH concentration is highest.

Atmospheric CO concentrations are measured at surface sites around the world. The limited measurements available before 1990 suggested that CO mole fractions in the Northern Hemisphere increased by 1–2 ppb/yr from the 1950s to the 1990s largely due to increases in fossil fuel combustion [*Khalil and Rasmussen*, 1984, 1988; *Levine et al.*, 1985], with little or no trend in the Southern Hemisphere. With the exception of atmospheric perturbations due to the 1991 eruption of Mount Pinatubo and the 1997/1998 El Niño, Northern Hemisphere CO decreased steadily (-0.92 ± 0.15 ppb/r) from the 1990s to 2001 [*Novelli et al.*, 2003]. Model interpretation of observed changes of CO at high northern latitudes (30–90°) during 1988–1997 show that the negative trend in mean annual CO mole fraction data was due to decreases in European fossil fuel emissions [*Duncan and Logan*, 2008]. A study based on measurements made in central Oregon, USA, reported a significant decrease

in mean springtime values of CO (−3.2 ± 2.9 ppb/yr) [*Gratz et al.*, 2015]. This decrease was similar to those determined at three NOAA sites over the North Pacific region (Midway, Mauna Loa, and Shemya). *Gratz et al.* [2015] tentatively link these changes to anthropogenic emissions from East Asia, Europe, and North America based on emission inventories. A recent study of CO mole fraction data collected on the Westman Islands, Iceland, between 2004 and 2009, found evidence of a decrease in CO mole fraction of 2.4 ± 1.1 ppb/yr [*Park et al.*, 2015], which uses coincident δ^{13}C and δ^{18}O measurements they attribute to changes in natural and anthropogenic sources. In this paper we examine specifically CO trends in the Arctic, which represent large-scale changes in high northern latitudes.

It is nontrivial to attribute observed atmospheric CO variations to specific processes. To address this we use two methods: (1) a wavelet transform to spectrally decompose the mole fraction data to study how characteristic periodic variations change with time and (2) a global 3-D atmospheric chemistry transport model to attribute observed variations to specific geographical regions. Previous analyses of the CO mole fraction time series used a smoothing function that represented the seasonal cycle by four harmonics and the trend as a polynomial [*Novelli et al.*, 2003; *Gratz et al.*, 2015]. The wavelet transform allows us to identify simultaneously the dominant modes of variability and how they change with time.

2. Data and Methods

2.1. CO Mole Fraction Data

We use the CO dry air mole fractions measured by flask air samples collected by the National Oceanic and Atmospheric Administration (NOAA) Cooperative Air Sampling Network. Air samples were collected approximately weekly under conditions believed representative of the large and well-mixed regional atmosphere. We focus our analysis on three Arctic sites: (1) Barrow, Alaska (BRW, 71°N, 157°W) from 1989 to 2012; (2) Alert, Nunavut, Canada (ALT, 82°N, 63°W) from 1992 to 2012; and (3) Zeppelin, Svalbard, Norway (ZEP, 79°N, 12°E) from 1994 to 2012. These sites were chosen for their long available data sets and strong seasonal cycle. By virtue of their location they should be able to observe any large-scale changes in the Northern Hemisphere atmosphere. Individual measurement uncertainty estimates for CO, accounting for collection, analysis, and calibration errors, are 2.8 ppb for the years 1989–2004.5, 1.1 ppb for the years 2004.5–2008.5, and 0.7 ppb from 2008.5 onward.

We focus our analysis on a weekly time series so that we minimize errors due to imputation while retaining observed changes on submonthly scales that would otherwise be lost. We prepare the weekly time series in two steps. First, we discard data that have been flagged by quality criteria [*Novelli and Masarie*, 2014]. Data collected within a calendar week are averaged and assigned to the midpoint of the week. Second, we impute the data gaps using two methods. We calculate a local temporal average from the three previous and three subsequent years at the times of any missing data, implicitly assuming that the time series is similar, or smoothly varying, from year to year with no abrupt trend. This is a reasonable assumption because the measurements are located such that they sample large-scale changes in CO and not local variations. This imputation is only used if these three previous and subsequent data points are not themselves missing. This mean was taken over 6 years as a compromise between retaining short-term variations and long-term trends. Any remaining data gaps are imputed using a cubic spline. The first imputation accounts for 11, 19, and 13% of the weekly data points for ALT, BRW, and ZEP, respectively, while the second accounts for 3, 5, and 4%. Figure 1 shows the original and imputed weekly mole fraction data at BRW. We show below that these imputed data do not significantly affect our reported results.

We also report annual and seasonal average CO concentrations. For each site we average the imputed weekly data record over a calendar year and assign that value to the midpoint of that year. We report the slope of a linear regression to represent a best fit line and the average of the upper and lower 95% confidence intervals to be the associated uncertainty. We use the conventional seasonal definitions: March–May (MAM), June–August (JJA), September–November (SON), and December–February (DJF), discarding incomplete seasons at the beginning and end of the time series. We average all weekly points within each season, assign that to the midpoint of the seasons, and use that information for the seasonal linear regression.

2.2. Wavelet Transform

We use a wavelet transform to spectrally decompose the weekly averaged CO mole fraction data:

$$W_n(s) = \sum_{n'=1}^{N-1} x_n \psi^* \left[\frac{(n'-n)\delta t}{s} \right], \quad (1)$$

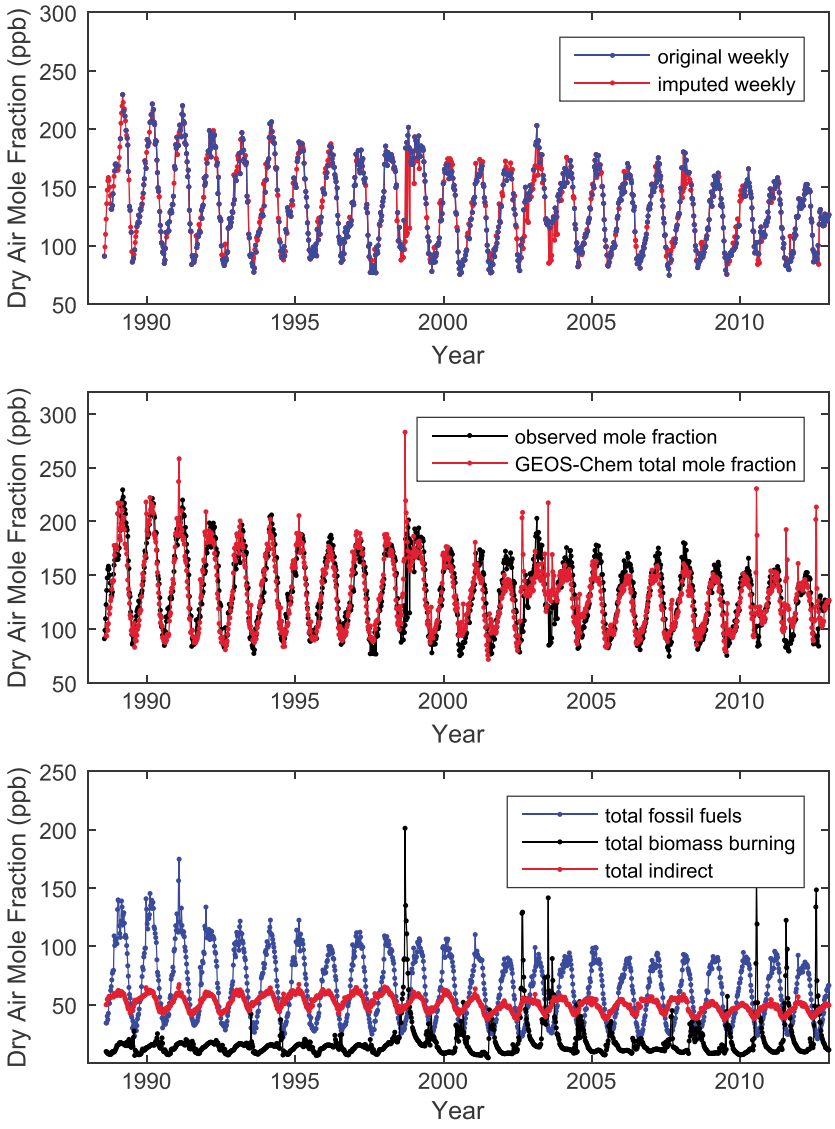

Figure 1. (top) The weekly NOAA CO mole fractions collected from Barrow, Alaska (BRW) between 1989 and 2012 and our imputed weekly data product that fills in data gaps necessary for the wavelet transform. (middle) Observed and GEOS-Chem model (1989–2012) weekly averaged CO mole fraction data. (bottom) The weekly averaged contributory global, linear tagged tracers of CO from fossil fuel combustion, biomass burning, and the secondary chemical source.

where ψ^* is the complex conjugate of the normalized form of the wavelet, δt is the time interval, x_n is the data, n is the time index, and s is the scale. The resulting power spectrum is shown in Figure 2. The region beneath the cone of influence (COI), faded in the figure, denotes regions where there may be edge effects, though these uncertainties have been minimized by padding the data. The advantage of this approach is that it preserves frequency variations as a function of time, allowing for the time evolution of signals, while not suffering from overrepresentation of high-frequency components like windowed Fourier transform methods [*Lau and Weng*, 1995]. Below we use the wavelet transform as a band-pass filter to isolate a subset of periods, e.g., to deseasonalize the model and data by retaining periods >18 months. We refer the reader to *Barlow et al.* [2015] for a more detailed mathematical discussion of this approach including values of the parameters used. By using equation (1), the weekly time series can be decomposed and reconstructed to within less than 1% of the original time series.

Based on the power spectrum of the spectrally decomposed CO data, we contend that periods of less than 6 months represent high-frequency variations most likely localized in space and time and consequently are not examined further. We determine the maxima and minima of the time series using the smoothed data

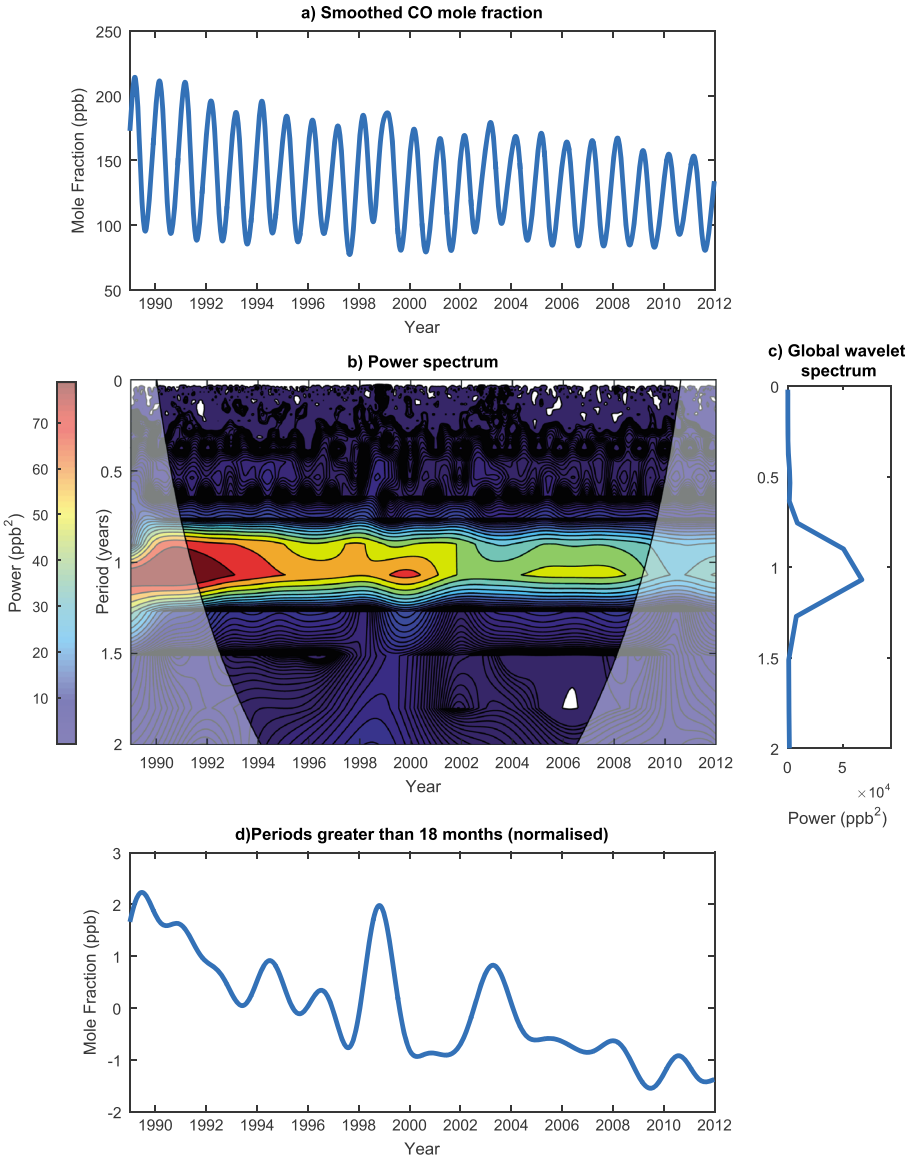

Figure 2. (a) Atmospheric CO mole fraction (ppb) at Barrow, Alaska, 1989–2012, with periods less than 6 months removed. (b) The wavelet power spectrum of that data, where the contours scale is power: blue indicates low power and red high power. Values that sit below the cone of influence (faded) may be affected by edge effects, therefore have a higher uncertainty. (c) The associated global wavelet power spectrum. (d) Periods longer than 18 months, which represent long-term variations representative of the atmospheric growth rate of CO.

(with periods of less than 6 months removed). We use periods between 6 and 18 months to describe the power associated with the detrended seasonal cycle. We define the amplitude of this detrended seasonal cycle to be the difference in concentration between a maxima and the following minima. Periods longer than 18 months represent long-term variations, representative of the atmospheric growth rate of CO. We calculate trends in the amplitude of the detrended seasonal cycle and the maxima and minima of the smoothed data using a linear regression. Using a Monte Carlo approach, we find that our reported trends are largely insensitive to perturbations of the data (represented by the product of $\mathcal{N}(-1, 1)$ and the estimated measurement uncertainty). Using a similar approach but only perturbing the imputed values, we find that even inflating the estimated measurement uncertainty by a factor of 10 does not significantly affect our reported results.

2.3. GEOS-Chem Global 3-D Chemistry Transport Model

To relate geographical sources of CO to observed atmospheric mole fractions we use v9-01-03 of the GEOS-Chem global chemistry transport model driven by MERRA analyzed meteorology provided by the

Table 1. Annual and Seasonal Mean Statistics Associated With the Linear Regression of CO Mole Fraction Data at NOAA Sites ALT (1992–2012), BRW (1989–2012), and ZEP (1994–2012)

		Observations			GEOS-Chem		
	Site	r^2	*p* Value	Slope (ppb/yr)	r^2	*p* Value	Slope (ppb/yr)
Annual avg.	ALT	0.47	0.0008	-1.0 ± 0.5	0.50	0.0005	-1.2 ± 0.6
	BRW	0.71	<0.0001	-1.2 ± 0.3	0.49	0.0001	-1.1 ± 0.5
	ZEP	0.44	0.003	-1.0 ± 0.6	0.47	0.002	-1.3 ± 0.7
MAM	ALT	0.71	<0.0001	-1.5 ± 0.4	0.75	<0.0001	-1.7 ± 0.5
	BRW	0.86	<0.0001	-1.9 ± 0.3	0.83	<0.0001	-1.9 ± 0.4
	ZEP	0.60	0.0001	-1.3 ± 0.5	0.68	<0.0001	-1.7 ± 0.6
JJA	ALT	0.10	0.2	-0.3 ± 0.4	0.04	0.4	0.3 ± 0.7
	BRW	0.34	0.002	-0.5 ± 0.3	0.21	0.02	0.8 ± 0.7
	ZEP	0.13	0.1	-0.4 ± 0.6	0.00	0.87	-0.1 ± 0.8
SON	ALT	0.08	0.21	-0.7 ± 1.1	0.13	0.12	-0.8 ± 1.0
	BRW	0.23	0.02	-0.9 ± 0.7	0.09	0.15	-0.7 ± 0.9
	ZEP	0.14	0.1	-0.9 ± 1.2	0.15	0.11	-1.0 ± 1.2
DJF	ALT	0.75	<0.0001	-1.7 ± 0.5	0.77	<0.0001	-2.3 ± 0.6
	BRW	0.80	<0.0001	-1.9 ± 0.4	0.86	<0.0001	-2.7 ± 0.5
	ZEP	0.73	<0.0001	-1.8 ± 0.6	0.68	<0.0001	-2.4 ± 0.9

Global Modeling and Assimilation Office at NASA Goddard [*Rienecker et al.*, 2011]. We use the meteorological data at a spatial resolution of 2° latitude by 2.5° longitude, with 47 vertical levels and run the model from January 1980 to March 2015, including a 9 month spin up to minimize the effect of initial conditions.

We use the tagged CO version of the model [*Bey et al.*, 2001; *Duncan et al.*, 2007; *Jones et al.*, 2003; *Palmer et al.*, 2003, 2006; *Fisher et al.*, 2010; *Finch et al.*, 2014], which uses precalculated 3-D OH fields, allowing us to linearly decompose the CO contributions from individual sources and particular geographical regions. For this experiment, we tag regions for fossil fuel and biofuel that immediately affect our measurement sites: North America (24–88°N, 18–100°W), Europe (35–88°N, 18°W–30°E), and East Asia (8–50°N, 70–155°E). The remaining globe is combined as the "rest of world" (ROW). For all purposes the ROW in the Northern Hemisphere represents Russia because the atmospheric lifetime of CO is much less than the typical interhemispheric transport time. We also include a tracer that describes the indirect CO source from the oxidation of methane and nonmethane volatile organic compounds [*Duncan et al.*, 2007].

We use the EDGAR global fossil fuel emission inventory developed by *Olivier et al.* [1999] except for East Asia, which we overwrite with country-specific values from *Zhang et al.* [2009] which have a seasonal variability applied to them. We use scaling factors 1985–2010 from both emission data sets [*van Donkelaar et al.*, 2008]. Emissions for pre-1985 and post-2010 years are adjusted using the 1985 and 2010 scaling factors, respectively. We use monthly biomass burning emission estimates 1997–2011 from *Giglio et al.* [2010]; estimates outside of these years are taken from the nearest year available. We use climatological biofuel emissions from *Yevich and Logan* [2003], and biogenic emissions that depend on meteorological drivers *Guenther et al.* [2006]. We sample the model at the time and location of the measurements and analyze them as we do the measurements.

3. Results

Figure 2 shows clearly that there is a downward trend in CO mole fraction at BRW and that the amplitude of the seasonal cycle is decreasing. The largest spectral power is associated with the seasonal cycle, as expected, though over a range of periods from 6 to 18 months. Table 1 shows the mean annual and seasonal statistics associated with the weekly CO mole fraction data. We find a significant negative annual trend in CO at BRW, ALT, and ZEP of 1.2 ± 0.3, 1.0 ± 0.5, and 1.0 ± 0.6 ppb/yr, respectively, over the past two decades. The two anomalies to this secular trend in 1998 and 2003 coincide with the El Niño phase of the El Niño-Southern Oscillation. The associated seasonal statistics at BRW, ALT, and ZEP are very different for different seasons, with the largest and the most statistically significant trends during MAM and DJF. Figure 1 shows the weekly averages from the model in comparison to the observations. The model reproduces the observations well

Table 2. Mean Statistics Associated With the Detrended Seasonal Cycle of CO Mole Fraction Data at NOAA Sites ALT (1992–2012), BRW (1989–2012), and ZEP (1994–2012)

		Observations			GEOS-Chem		
	Site	r^2	*p* Value	Slope (ppb/yr)	r^2	*p* Value	Slope (ppb/yr)
Amp.	ALT	0.81	<0.0001	−1.9 ± 0.5	0.69	<0.0001	−3.4 ± 1.2
	BRW	0.86	<0.0001	−2.3 ± 0.4	0.78	<0.0001	−4.5 ± 1.1
	ZEP	0.54	0.004	−1.2 ± 0.7	0.61	0.0001	−2.9 ± 1.2
Max.	ALT	0.82	<0.0001	−2.0 ± 0.5	0.82	<0.0001	−2.8 ± 0.7
	BRW	0.88	<0.0001	−2.4 ± 0.4	0.86	<0.0001	−3.2 ± 0.5
	ZEP	0.70	<0.00001	−1.5 ± 0.5	0.73	<0.0001	−2.7 ± 0.9
Min.	ALT	0.01	0.6	−0.2 ± 0.7	0.04	0.4	0.4 ± 1.0
	BRW	0.08	0.3	−0.3 ± 0.4	0.09	0.1	1.0 ± 1.3
	ZEP	0.07	0.3	−0.5 ± 1.0	0.00	0.8	0.1 ± 1.0

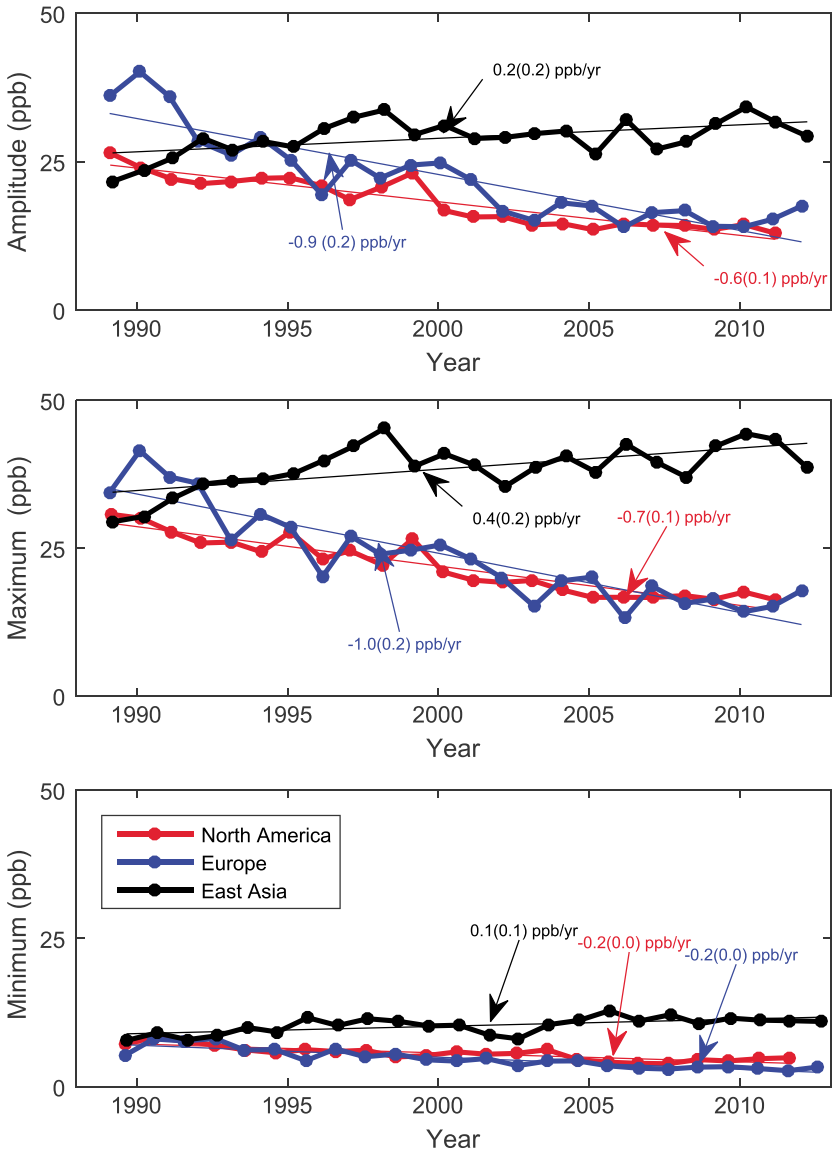

Figure 3. GEOS-Chem model trends in the amplitude, maximum, and minimum of contributions from regional fossil fuel sources to CO mole fractions at BRW from 1989 to 2012. Table 3 shows the associated numerical values.

Table 3. Statistics Associated With the Detrended Seasonal Cycle of CO Mole Fraction From Fossil Fuel Emissions From GEOS-Chem at NOAA Sites ALT (1992–2012), BRW (1989–2012), and ZEP (1994–2012)

	Site	Origin	r^2	p Value	Slope (ppb/yr)
Amp.	ALT	NA	0.82	<0.0001	−0.4 ± 0.1
		EU	0.86	<0.0001	−0.8 ± 0.2
		EA	0.13	0.1	0.1 ± 0.2
		ROW	0.17	0.07	−0.1 ± 0.2
	BRW	NA	0.86	<0.0001	−0.6 ± 0.1
		EU	0.79	<0.0001	−0.9 ± 0.2
		EA	0.29	0.006	0.2 ± 0.2
		ROW	0.44	0.0004	−0.8 ± 0.4
	ZEP	NA	0.71	<0.0001	−0.3 ± 0.1
		EU	0.57	0.0003	−0.8 ± 0.4
		EA	0.00	0.8	0.0 ± 0.2
		ROW	0.02	0.6	0.1 ± 0.2
Max.	ALT	NA	0.89	<0.0001	−0.5 ± 0.1
		EU	0.80	<0.0001	−1.0 ± 0.2
		EA	0.14	0.1	0.4 ± 0.2
		ROW	0.12	0.1	−0.1 ± 0.2
	BRW	NA	0.89	<0.0001	−0.7 ± 0.1
		EU	0.80	<0.0001	−1.0 ± 0.2
		EA	0.41	0.0007	0.4 ± 0.2
		ROW	0.44	0.0004	−0.7 ± 0.4
	ZEP	NA	0.84	<0.0001	−0.5 ± 0.1
		EU	0.66	<0.0001	−1.1 ± 0.4
		EA	0.03	0.5	0.1 ± 0.2
		ROW	0.01	0.7	0.0 ± 0.3
Min.	ALT	NA	0.70	<0.0001	−0.2 ± 0.0
		EU	0.77	<0.0001	−0.2 ± 0.1
		EA	0.10	0.2	0.0 ± 0.1
		ROW	0.05	0.5	0.0 ± 0.0
	BRW	NA	0.73	<0.0001	−0.2 ± 0.0
		EU	0.76	<0.0001	−0.2 ± 0.0
		EA	0.39	0.001	0.1 ± 0.1
		ROW	0.21	0.03	−0.0 ± 0.0
	ZEP	NA	0.69	<0.0001	−0.2 ± 0.1
		EU	0.65	<0.0001	−0.3 ± 0.1
		EA	0.11	0.2	0.1 ± 0.1
		ROW	0.02	0.6	0.0 ± 0.1

with a squared Pearson correlation coefficient (r^2) of 0.77, 0.66, and 0.70 for ALT, BRW, and ZEP, respectively. The model also reproduces the longer-term variations (periods of 18 months and over) in the observations well, with $r^2 = 0.85$, 0.80, and 0.81 for the three sites, respectively. We find that the measured and model CO mole fraction show statistically significant negative trends in observed seasonal mean concentrations of CO at all sites during DJF and MAM, but not during JJA and SON (Table 1). Trends determined by the model are generally larger than observed values by typically 0.2–0.3 ppb/yr in summer, spring, and fall but reaching 0.8 ppb/yr during DJF.

Table 2 shows the trend analysis statistics of the maxima and minima after high-frequency variations (periods of 6 months or less) have been removed, and the amplitude of the isolated seasonal cycle (periods 6–18 months), both done with the wavelet analysis. Table 2 shows that these trends result from a large,

significant decrease in the seasonal cycle maximum, with no significant change to the depth of the summer minima. The model overestimates by a factor of 2 the observed negative trend in the amplitude of the detrended seasonal cycle, although values are generally consistent within the associated uncertainty bounds. The model also overestimates the observed trends in the maxima and minima but to a lesser extent.

Figure 1 shows using the GEOS-Chem global 3-D atmospheric chemistry and transport model that modeled changes in Arctic CO mole fraction are consistent with a reduction in the emissions from fossil fuel combustion. Biomass burning has a seasonal contribution, peaking in the spring and summer months, with anomalously large values associated with El Niño. The CO source from the oxidation of methane and nonmethane volatile organic compounds is small compared to fossil fuel combustion for the majority of the annual cycle, but its proportional contribution is increasingly becoming more important as the combustion source decreases.

Figure 3 (for BRW) and Table 3 (for all sites) show that the trends in the amplitude and maxima of the modeled CO mole fractions are driven by a steady decline in the modeled fossil emissions transported from North America and Europe. At these sites, the contribution from East Asia increases, resulting in a small compensating effect on the total CO. The trends in the minima for North America and Europe are small and negative, while for East Asia the trend is small and positive but not statistically significant.

We calculate regional trends in annual emissions from 1989 to 2012 used in GEOS-Chem by region, which show statistically significant negative trends for CO in North America and Europe of -2.4 ± 0.3 Tg yr^{-1} and -2.3 ± 0.2 Tg yr^{-1} respectively, and a positive trend of 2.9 ± 1.1 Tg yr^{-1} from East Asia. In a separate study, the TM5 model was used to analyze atmospheric CH_4 mole fraction at these Arctic sites (L. Bruhwiler, personal communication, 2016). Using a series of model calculations, the study showed that atmospheric transport introduced year-to-year variations in atmospheric CH_4 but no trend. This suggests that observed CO mole fraction trends in the Arctic can be largely attributed to changes in emissions rather than atmospheric transport.

Our work builds on a previous study that showed that atmospheric CO decreased in the high northern hemisphere (30–90°) over 1988–1997 due to reduced European emissions [*Duncan and Logan*, 2008], with compensatory increasing Asian emissions having less of an impact at the higher northern latitude sites due to predominately westward transport pathways. Our study has analyzed the data over a longer duration, allowing us to use more advanced statistical machinery with confidence.

4. Concluding Remarks

In a changing Arctic environment, driven by coupled anthropogenic and natural processes, it may be possible to detect subtle variations in frequency and time using a more broadly defined seasonal cycle rather than changes in annual or seasonal means as commonly studied. As such, spectral decomposition of data offers a much richer approach for detecting changes in atmospheric chemistry, by allowing for nonstationary processes. Here we focused our analysis on CO mainly because of the availability of long measurement records over the Arctic, but to a limited extent we expect to be able to relate our findings to other trace gases and particulate matter that share common midlatitude sources [*Quinn et al.*, 2007], which determine the observed variations in the maximum of the seasonal cycle. However, during summer months, variations in the seasonal minimum of CO and particulate matter are due to different physical and chemical processes.

Acknowledgments
We thank NOAA/ESRL for the CO surface mole fraction data which are provided by NOAA/ESRL PSD, Boulder, Colorado, USA, from their website http://www.esrl.noaa.gov/psd/. We would also like to thank Torrence and Compo (1998) for making the wavelet transform code freely available at the website http://paos.colorado.edu/research/wavelets/software.html. We thank the GEOS-Chem support team at Harvard University, Dalhousie University, and University of Colorado. J.M. Barlow acknowledges the Centre for Earth Observation Instrumentation and the National Environmental Research Council for funding his studentship, NE/1528818/1. P.I. Palmer acknowledges his Royal Society Wolfson Research Merit Award. A.R.M. and P.I.P. designed the experiments and wrote the paper. A.R.M. conducted the wavelet analysis with support from J.M.B., and D.P.F. performed the GEOS-Chem model calculation. P.N. provided access to unpublished data and advice on using these data. P.N. and L.J. provided input to the writing process.

References

Barlow, J. M., P. I. Palmer, L. M. Bruhwiler, and P. Tans (2015), Analysis of CO_2 mole fraction data: First evidence of large-scale changes in CO_2 uptake at high northern latitudes, *Atmos. Chem. Phys. Discuss.*, *15*(5), 7089–7139, doi:10.5194/acpd-15-7089-2015.

Bey, I., D. J. Jacob, R. M. Yantosca, J. A. Logan, B. D. Field, A. M. Fiore, Q. Li, H. Y. Liu, L. J. Mickley, and M. G. Schultz (2001), Global modeling of tropospheric chemistry with assimilated meteorology: Model description and evaluation, *J. Geophys. Res.*, *106*(D19), 23,073–23,096, doi:10.1029/2001JD000807.

Derwent, R., P. Simmonds, S. Seuring, and C. Dimmer (1998), Observation and interpretation of the seasonal cycles in the surface concentrations of ozone and carbon monoxide at Mace Head, Ireland from 1990 to 1994, *Atmos. Environ.*, *32*(2), 145–157, doi:10.1016/S1352-2310(97)00338-5.

Duncan, B. N., and J. A. Logan (2008), Model analysis of the factors regulating the trends and variability of carbon monoxide between 1988 and 1997, *Atmos. Chem. Phys.*, *8*(24), 7389–7403, doi:10.5194/acp-8-7389-2008.

Duncan, B. N., J. A. Logan, I. Bey, I. A. Megretskaia, R. M. Yantosca, P. C. Novelli, N. B. Jones, and C. P. Rinsland (2007), Global budget of CO, 1988–1997: Source estimates and validation with a global model, *J. Geophys. Res.*, *112*, D22301, doi:10.1029/2007JD008459.

Finch, D. P., P. I. Palmer, and M. Parrington (2014), Origin, variability and age of biomass burning plumes intercepted during BORTAS-B, *Atmos. Chem. Phys.*, *14*(24), 13,789–13,800, doi:10.5194/acp-14-13789-2014.

Fisher, J. A., et al. (2010), Source attribution and interannual variability of Arctic pollution in spring constrained by aircraft (ARCTAS, ARCPAC) and satellite (AIRS) observations of carbon monoxide, *Atmos. Chem. Phys.*, *10*(3), 977–996, doi:10.5194/acp-10-977-2010.

Giglio, L., J. T. Randerson, G. R. van der Werf, P. S. Kasibhatla, G. J. Collatz, D. C. Morton, and R. S. DeFries (2010), Assessing variability and long-term trends in burned area by merging multiple satellite fire products, *Biogeosciences*, *7*(3), 1171–1186, doi:10.5194/bg-7-1171-2010.

Gratz, L., D. Jaffe, and J. Hee (2015), Causes of increasing ozone and decreasing carbon monoxide in springtime at the Mt. Bachelor Observatory from 2004 to 2013, *Atmos. Environ.*, *109*, 323–330, doi:10.1016/j.atmosenv.2014.05.076.

Guenther, A., T. Karl, P. Harley, C. Wiedinmyer, P. I. Palmer, and C. Geron (2006), Estimates of global terrestrial isoprene emissions using MEGAN (Model of Emissions of Gases and Aerosols from Nature), *Atmos. Chem. Phys. Discuss.*, *6*(1), 107–173, doi:10.5194/acpd-6-107-2006.

Jones, D. B. A., K. W. Bowman, P. I. Palmer, J. R. Worden, D. J. Jacob, R. N. Hoffman, I. Bey, and R. M. Yantosca (2003), Potential of observations from the tropospheric emission spectrometer to constrain continental sources of carbon monoxide, *J. Geophys. Res..*, *108*(D24), 4789, doi:10.1029/2003JD003702.

Khalil, M. A., and R. A. Rasmussen (1984), Carbon monoxide in the Earth's atmosphere: Increasing trend, *Science*, *224*, 54–56.

Khalil, M. A., and R. A. Rasmussen (1988), Carbon monoxide in the Earth's atmosphere: Indications of a global increase, *Nature*, *332*, 242–245.

Levine, J. S., C. P. Rinsland, and G. M. Tennille (1985), The photochemistry of methane and carbon monoxide in the troposphere in 1950 and 1985, *Nature*, *318*, 254–257.

Lau, K.-M., and H. Weng (1995), Climate signal detection using wavelet transform: How to make a time series sing, *Bull. Am. Meteorol. Soc.*, *76*(12), 2391–2402.

Novelli, P. C., and K. A. Masarie (2014), Atmospheric carbon monoxide dry air mole fractions from the NOAA ESRL Carbon Cycle Cooperative Global Air Sampling Network, 1988–2013, version: 2014-07-02t.

Novelli, P. C., K. A. Masarie, P. M. Lang, B. D. Hall, R. C. Myers, and J. W. Elkins (2003), Reanalysis of tropospheric CO trends: Effects of the 1997–1998 wildfires, *J. Geophys. Res.*, *108*(D15), 4464, doi:10.1029/2002JD003031.

Olivier, J. G., J. P. J. Bloos, J. J. Berdowski, A. J. Visschedijk, and A. F. Bouwman (1999), A 1990 global emission inventory of anthropogenic sources of carbon monoxide on $1^{\circ} \times 1^{\circ}$ developed in the framework of EDGAR/GEIA, *Chemosphere Global Change Sci.*, *1*(1–3), 1–17, doi:10.1016/S1465-9972(99)00019-7.

Palmer, P. I., D. J. Jacob, D. B. A. Jones, C. L. Heald, R. M. Yantosca, and J. A. Logan (2003), Inverting for emissions of carbon monoxide from Asia using aircraft observations over the western Pacific, *J. Geophys. Res.*, *108*(D21), 8828, doi:10.1029/2003JD003397.

Palmer, P. I., P. Suntharalingam, D. B. A. Jones, D. J. Jacob, D. G. Streets, Q. Fu, S. A. Vay, and G. W. Sachse (2006), Using CO_2: CO correlations to improve inverse analyses of carbon fluxes, *J. Geophys. Res.*, *111*, D12318, doi:10.1029/2005JD006697.

Park, K., Z. Wang, L. K. Emmons, and J. E. Mak (2015), Variation of atmospheric CO, $\delta^{13}C$, and $\delta^{18}O$ at high northern latitude during 2004–2009: Observations and model simulations, *J. Geophys. Res. Atmos.*, *120*, 11,024–11,036, doi:10.1002/2015JD023191.

Quinn, P. K., G. Shaw, E. Andrews, E. G. Dutton, T. Ruoho-Airola, and S. L. Gong (2007), Arctic haze: Current trends and knowledge gaps, *Tellus B*, *59*, 99–114.

Rienecker, M. M., et al. (2011), MERRA: NASA's modern-era retrospective analysis for research and applications, *J. Clim.*, *24*(14), 3624–3648, doi:10.1175/JCLI-D-11-00015.1.

Shindell, D. (2007), Local and remote contributions to Arctic warming, *Geophys. Res. Lett.*, *34*, L14704, doi:10.1029/2007GL030221.

Stocker, T., D. Qin, G.-K. Plattner, M. Tignor, S. Allen, J. Boschung, A. Nauels, Y. Xia, V. Bex, and P. Midgley (Eds.) (2013), *Summary for Policymakers*, pp. 1–30, Cambridge Univ. Press, Cambridge, U. K., and New York, doi:10.1017/CBO9781107415324.004.

van Donkelaar, A., et al. (2008), Analysis of aircraft and satellite measurements from the Intercontinental Chemical Transport Experiment (INTEX-B) to quantify long-range transport of East Asian sulfur to Canada, *Atmos. Chem. Phys.*, *8*(11), 2999–3014, doi:10.5194/acp-8-2999-2008.

Yevich, R., and J. A. Logan (2003), An assessment of biofuel use and burning of agricultural waste in the developing world, *Global Biogeochem. Cycles*, *17*(4), 1095, doi:10.1029/2002GB001952.

Zhang, Q., et al. (2009), Asian emissions in 2006 for the NASA INTEX-B mission, *Atmos. Chem. Phys.*, *9*(14), 5131–153, doi:10.5194/acp-9-5131-2009.